Pore Engineering of MFI Zeolite Membranes: Enhancing Water Flux and Ion Rejection Using Polyacrylamide as a Secondary Template

R. Shahbaz and M. J. Vaezi[*]

Nanostructure Material Research Center (NMRC), Chemical Engineering Faculty, Sahand University of Technology, P.O.Box 53318-17634, Tabriz, Iran

A mesoporous MFI zeolite membrane was synthesized using polyacrylamide as a secondary template to separate nickel, chromium, and nitrate ions from water. Various analytical methods were employed to characterize the zeolite powders and membranes. Subsequently, tests were conducted to evaluate water permeation and the rejection of heavy metals and nitrate ions. The incorporation of 0.03 kg kg^{-1} polyacrylamide resulted in a 90 % mesostructure in the MFI zeolite. Higher amounts of polymer had no positive effect on the mesoporous structure. The membrane demonstrated a high water flux (22 L m^{-2} h^{-1}) with 99 % nickel and 93 % chromium rejection, and effective nitrate rejection (up to 34 %). Increasing the total dissolved solids from 1 to 1000 μA A^{-1} led to a 50 % increase in water flux. Additionally, raising the pressure by 2 bar resulted in an 80 % increase in the water flux and 15 % improvement in nitrate rejection.

Keywords
MFI zeolite membrane, secondary template, polyacrylamide, mesoporous structure, ion rejection

Introduction

Population growth and technological progress have led to increased water consumption and significant water pollution, which adversely affects living organisms[1]. Among the pollutants in water sources are heavy metal ions, which have various detrimental effects on human health, plants, and aquatic life. Several methods exist for removing heavy metal ions from water, including chemical precipitation, ion exchange, membrane separation, reverse osmosis, and electrocoagulation[2]. Among these, membrane separation stands out as a promising technique. Zeolites, as candidates for membrane preparation, offer high adsorption capacity, molecular sieving effects, and ion exchange properties. Consequently, zeolites are used industrially for separating linear from nonlinear hydrocarbons, removing heavy metal ions from water, reducing ammonium levels in ammonium-containing water, and gas adsorption and separation. Zeolite membranes have been synthesized on various supports and are particularly effective in liquid separations[3]. However, many zeolitic membranes studied for water purification[4–12] have lost popularity due to low water flux. Moreover, none of these studies has focused on heavy metal ion separation. Among zeolite membranes, the all-silica MFI zeolite structure demonstrates excellent stability under harsh operating conditions, making it a suitable candidate for further investigation to enhance permeation rates. Creating a mesoporous structure within the zeolite membrane layer could be an effective method to increase the water permeation rate through zeolite membranes.

Despite extensive research on creating mesoporous structures in zeolite powders for catalytic applications, no studies have focused on developing mesoporous structures within zeolite membrane layers. Methods for creating mesoporous structures include post synthesis approaches and secondary templating during hydrothermal synthesis. Dealumination and silica extraction are among the most common post-synthesis methods used to increase the pore size of MFI zeolites[13–15]. For example, Van Oers *et al.*[13] achieved mesoporous structures with surface areas ranging from 99 m^2 g^{-1} to 259 m^2 g^{-1} in beta zeolite through dealumination, representing 50 % to 73 % mesoporous content. Similarly, Ogura *et al.*[15], and Verboekend *et al.*[14] utilized the silica extraction method to create mesoporous structures in ZSM-5 and silicalite-1 zeolites, achieving mesoporous contents of 67 % and 70 %, with mesopore surface areas of 115 m^2 g^{-1} and 182 m^2 g^{-1}, respectively. However, these extraction methods are limited by the need for strong acids and water to reduce the acidity of the resulting solution after use. In

---
[*]Corresponding author: E-mail address: m_vaezi@sut.ac.ir (m.j. vaezi), Tel.: +984133459170; Fax: +984133444355.

contrast, the secondary template method allows for the straightforward creation of mesoporous structures in various zeolite types[16]. The surface area and volume of mesopores created by secondary templating are competitive compared to those created by post-synthesis methods[17]. For instance, Abdulridha *et al.*[18] used the secondary templating method to achieve an 80 % mesoporous structure for FAU zeolite, with a mesopore surface area of 347 m^2 g^{-1}. These results demonstrate the potential of the secondary templating method for creating a high mesoporous content in zeolites. Templates used in this process can be categorized into hard and soft types. Hard templates act as physical barriers during zeolite synthesis, allowing zeolites to replicate their morphology. Soft templates, typically polymers, are less effective at space confinement but significantly influence zeolite nucleation and growth through molecular interactions with zeolite precursors. The combination of space confinement and molecular interactions in polymer networks provides greater control over zeolite synthesis[19]. Currently, the most commonly used templates for mesoporous zeolites are polymers (especially cationic polymers), silane organic acids, alkyl aluminum, and alkylphosphonates with long chains[20].

Among polymer materials, polyacrylamide (PAM) can be used as a soft secondary template for modifying zeolite structures. PAM has been used to synthesize α-alumina supports with various porosities via the gel casting method. Therefore, this research aimed to use polyacrylamide as a secondary template to create mesoporous structures in MFI zeolite powder and subsequently in MFI zeolite membranes to increase water permeation rates. To achieve this objective, various characterization techniques, such as X-ray diffraction (XRD), Brunauer-Emmett-Teller (BET) nitrogen adsorption studies, derivative thermogravimetry – thermogravimetric analysis (DTG-TGA), transmission electron microscopy (TEM), field emission scanning electron microscopy (FESEM), and energy dispersive X-ray analysis (EDX), were employed to analyze the synthesized zeolite powders and membranes. The separation performance of the synthesized membrane for heavy metal ions and nitrate removal from contaminated water was evaluated using water permeation tests and atomic absorption spectroscopy (AAS) and ultraviolet spectroscopy (UV) analyses.

Experimental

Materials

Tetraethyl orthosilicate (TEOS, $C_8H_{20}O_4Si$, > 98 %, Samchun), tetrapropylammonium bromide (TPABr, $(CH_3CH_2CH_2)_4N(Br)$, > 99 %, Merck) and sodium hydroxide (NaOH, > 99 %, Merck) were used as the silica source, primary template (structure directing agent), and mineralizing agent, respectively, in the synthesis of the MFI zeolite. Polyacrylamide (PAM, $(C_3H_5NO)_n$, > 95 %, 1500 g mol^{-1}, Merck) was used as a secondary template to create a mesoporous structure in the MFI zeolite.

Synthesis of mesoporous MFI zeolite powder

The mesoporous MFI zeolite powder was synthesized by combining two solutions. The first solution contained water, sodium hydroxide, TEOS, and TPABr, while the second solution consisted of polyacrylamide and water. The first solution was initiated by dissolving a specified amount of sodium hydroxide in water for 30 minutes, followed by the dropwise addition of TEOS. After 1 hour, TPABr was added, and the solution was stirred for another hour. The molar ratio of the components in the first solution was 1 TEOS : 0.4 NaOH : 0.2 TPABr : 135 H_2O. The second solution was prepared by dissolving a specific amount of polyacrylamide in a defined amount of water at 60 °C. Polyacrylamide was used with 0.03 kg kg^{-1} and 0.05 kg kg^{-1} dry precursors (TEOS, NaOH, and TPABr) in the first solution. The two solutions were then combined and stirred for 1 hour. The final mixture was transferred to a PTFE (polytetrafluoroethylene, Teflon) container and placed in an autoclave at 170 °C for 24 h. After hydrothermal treatment, the resulting powder was washed and dried at 110 °C for 4 h in an oven. The powders were then calcined at 550 °C for 4 h in an electric furnace to remove the primary and secondary templates. In this study, two zeolite powder samples were synthesized, designated as P1-TP-170-PAM-3 and P2-TP-170-PAM-5, containing 0.03 and 0.05 kg of PAM per kg of dry precursors (TEOS, NaOH and TPABr), respectively.

Synthesis of the mesoporous MFI zeolite membrane

The synthesis solution for the mesoporous MFI zeolite membrane was prepared following the same method as described for the powder synthesis. After preparation, a metal rod wrapped with Teflon tape was placed inside the tubular α-alumina support. The support was sealed on both sides of the rod with Teflon tape to prevent the synthesis solution from penetrating the support, thereby promoting crystal growth only on the external surface of the support. The prepared support was then placed in a PTFE holder, into which the synthesis solution was poured. The holder was placed inside an oven at 170 °C for 24 h. The synthesized membranes were washed with deionized water until the pH of the rinse water was neutral. Finally, the obtained mem-

branes were calcined in an electrical furnace at 550 °C for 4 h to remove the templates and complete the crystallization of the zeolite layer.

Characterization

X-ray diffraction (XRD) analysis was used to determine the crystalline structure of the synthesized samples. XRD patterns were obtained using a Philips PW1730 X-ray diffractometer under the following conditions: CuKα1 radiation with a wavelength (λ) of 1.5406 Å, 40 kV, 30 mA, and scanning at $2\theta = 10$–$40°$ at a rate of $0.05°$ s^{-1}. BET-BJH (Brunauer-Emmett-Teller/Barrett-Joyner-Halenda) analysis was performed with a Micromeritics, Asap2020 apparatus, USA, to measure the physical properties (surface area, volume, and pore size distribution) of the synthesized powders. DTG-TGA analysis was conducted using a Mettler Toledo instrument (TGA/SDTA 851 e, Switzerland) over a temperature range of 0 °C to 700 °C with a heating rate of 10 min °C^{-1} and N$_2$ purge gas. TEM images were obtained using a Philips EM 208S electron microscope with an accelerating voltage of 100 kV. For sample preparation, 5 mg of the powder was dispersed in 5 mL of water using an ultrasonic probe with a power of 300 W and placed inside the set. The surface morphology and cross-sectional structure of the synthesized membrane were investigated using a FESEM Tescan Mira3 apparatus, Czechia. For sample preparation, a part of the membrane was cut and broken by impact. One piece was used for surface analysis, while another was prepared for cross-sectional analysis by smoothing the lower part with sandpaper. The cross-sectional sample was placed on its side to capture images. Finally, the parts were coated with gold and placed in the set. The apparatus was equipped with an EDX detector, for qualitative and quantitative analysis.

A routine method for characterizing synthesized zeolite membranes involves gas permeation testing for pure gas. The absence of permeation flux through the synthesized zeolite layer confirms that the surface of the ceramic support is completely covered with zeolite crystals. For these measurements, the membranes were placed in a module under different pressures of pure gas, and the volumetric flow rate of the gas permeating through the membrane was measured using a bubble flow meter. The membrane permeance was subsequently calculated at 25 °C using the following equation (1):

Water permeation test and ion separation performance evaluation

To calculate the flux of deionized water and water containing ions (Ni^{2+}, Cr^{3+} and NO$_3^-$), the membrane was placed inside a test module, and water was introduced into the system. The module had two output streams: permeate (treated water) and retentate (untreated feed water). The flow rate of the permeate was recorded, along with the measurement time (Δt). The collected data were then used to calculate the permeate water flow rate using equation (2) as follows:

$$\text{Flux (L m}^{-2}\text{ h}^{-1}) = 2 \cdot V(\text{L})/[(\pi \cdot r(\text{m}) \cdot L(\text{m}) \cdot \Delta t(\text{h})] \quad (2)$$

where V is the volume of water (permeate stream) through the membrane during measurement time (Δt). L is the effective length of the membrane, and r is the radius of the membrane.

To measure the presence of heavy metal ions on the permeate side of the membrane, the membrane's separation performance was evaluated using AAS. The analysis was conducted using an AA220FS atomic absorption spectrometer (Varian, USA). Additionally, the concentration of nitrate ions on the permeate side of the membrane was measured using UV spectrophotometry at a wavelength of 220 nm.

Results and discussion

Characterization of mesoporous MFI zeolite powders

The crystalline structure of the MFI zeolite was confirmed by comparing the XRD patterns of the synthesized samples with the MFI reference pattern. Fig. 1 presents the XRD patterns of synthesized samples P1-TP-170-PAM-3 and P2-TP-170-PAM-5, alongside the MFI reference. A comparison of the XRD patterns with the reference confirmed the crystalline structure of the MFI zeolite in both samples, showing similarities at 2θ angles of $13°$ to $16°$, $23°$ to $25°$, and $30°$.

Fig. 2 shows the adsorption-desorption isotherms and pore size distributions of the synthesized MFI zeolite samples (P1-TP-170-PAM-3 and P2-TP-170-PAM-5). The hysteresis loops observed in the adsorption-desorption isotherms indicate the mesoporous structure of the synthesized zeolite
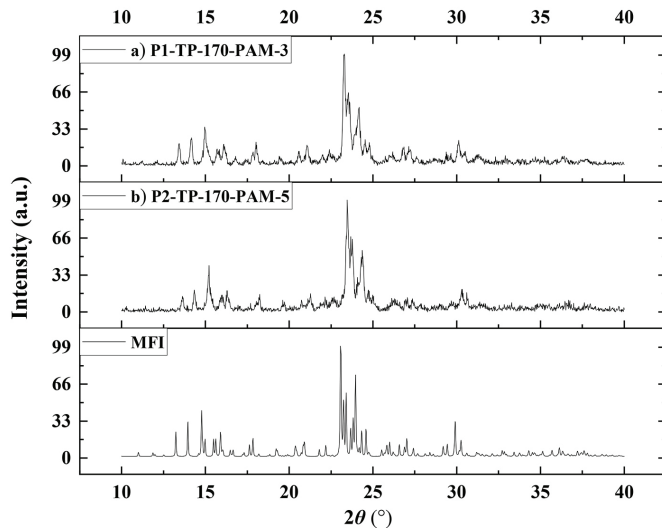
$$\text{Permeance (mol Pa}^{-1}\text{ s}^{-1}\text{ m}^{-2}) = 11 \cdot 10^{-6} \cdot V(\text{cm}^3)/[D(\text{mm}) \cdot L(\text{cm}) \cdot \Delta P(\text{bar}) \cdot \Delta t(\text{s})] \quad (1)$$

where V is the volume of gas permeating through the membrane, and D and L are the diameter and effective length of the membrane, respectively. ΔP is the pressure difference applied across the membrane. Δt is the measurement time required for a certain volume of gas to permeate.

F i g. 1 – *XRD patterns of the synthesized MFI zeolite samples: (a) P1-TP-170-PAM-3, (b) P2-TP-170-PAM-5, and MFI reference*

powders. The adsorption isotherms are type IV, and the hysteresis loops are type H1, indicating the presence of cylindrical or spherical mesopores in the structure. The variation in polymer percentage used in preparing the zeolite structure partially affected the total pore volume, with P2-TP-170-PAM-5 exhibiting slightly higher values than P1-TP-170-PAM-3. However, the pore size distribution remained consistent, with most pores measuring 2

nm in diameter. However, a significant difference was observed in the hysteresis regions of the nitrogen adsorption-desorption isotherms, especially for P1-TP-170-PAM-3. This suggested that increasing the polymer concentration in the synthesis solution had no positive effect on the amount of mesoporous structure created in the synthesized zeolite powder. Furthermore, a higher polymer content in the synthesis solution may hinder the formation of zeolite structures. Table 1 presents the BET analysis data for samples P1-TP-170-PAM-3 and P2-TP-170-PAM-5. The specific surface area, mesoporous surface area, and mesoporous volume of P1-TP-170-PAM-3 were slightly greater than those of P2-TP-170-PAM-5. The increase in mesoporous volume and surface area contributed to a higher percentage of mesoporosity in the structure of P1-TP-170-PAM-3.

DTG-TGA was conducted to evaluate the decomposition of the primary and secondary templates at various temperatures with a specific time step for the powder samples P1-TP-170-PAM-3 and microporous MFI zeolite (containing only the primary template). As shown in Fig. 3, both samples initially exhibited a rapid decreasing trend, indicating the presence of moisture in the structure. Moisture is the only component that can be quickly removed from a sample at initial and low temperatures. The microporous MFI zeolite powder underwent a sig-
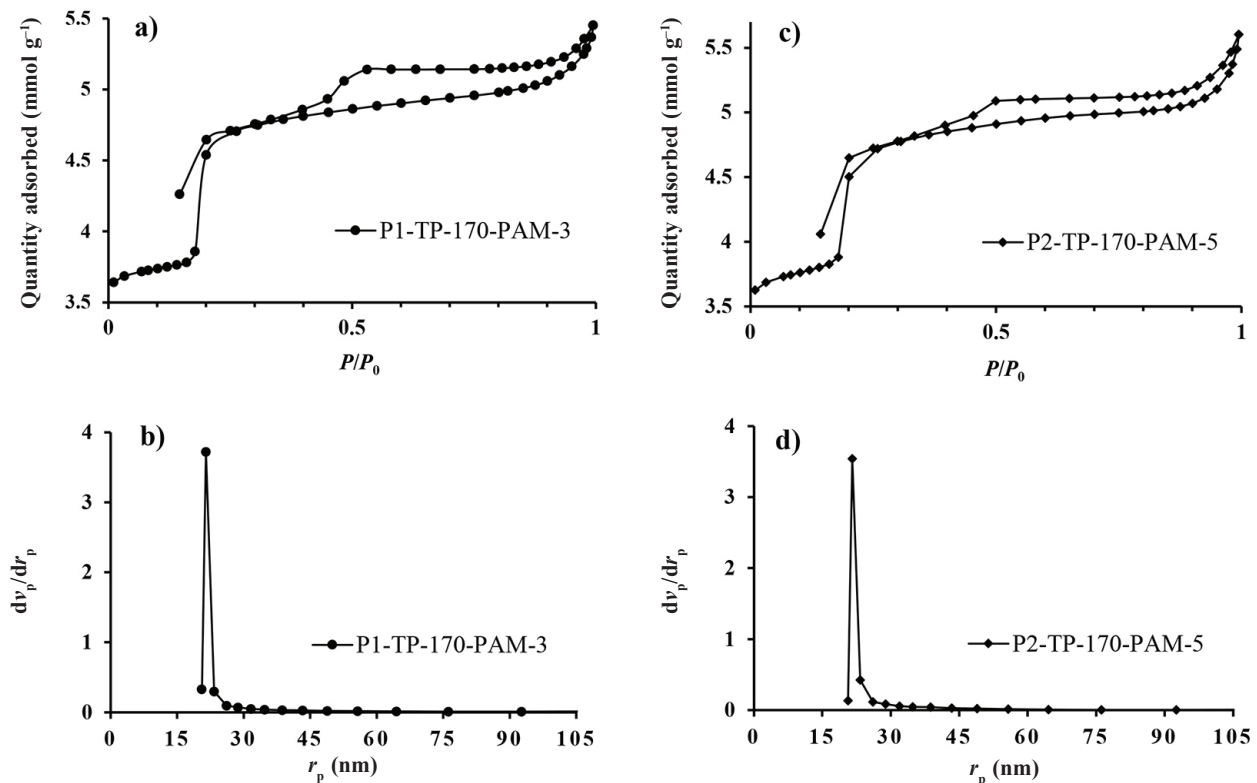

F i g. 2 – *Adsorption-desorption isotherms and pore size distributions of the synthesized MFI zeolite samples: (a, b) P1-TP-170-PAM-3 and (c, d) P2-TP-170-PAM-5*

Table 1 – *Structural properties of the MFI zeolite samples: P1-TP-170-PAM-3 and P2-TP-170-PAM-5*

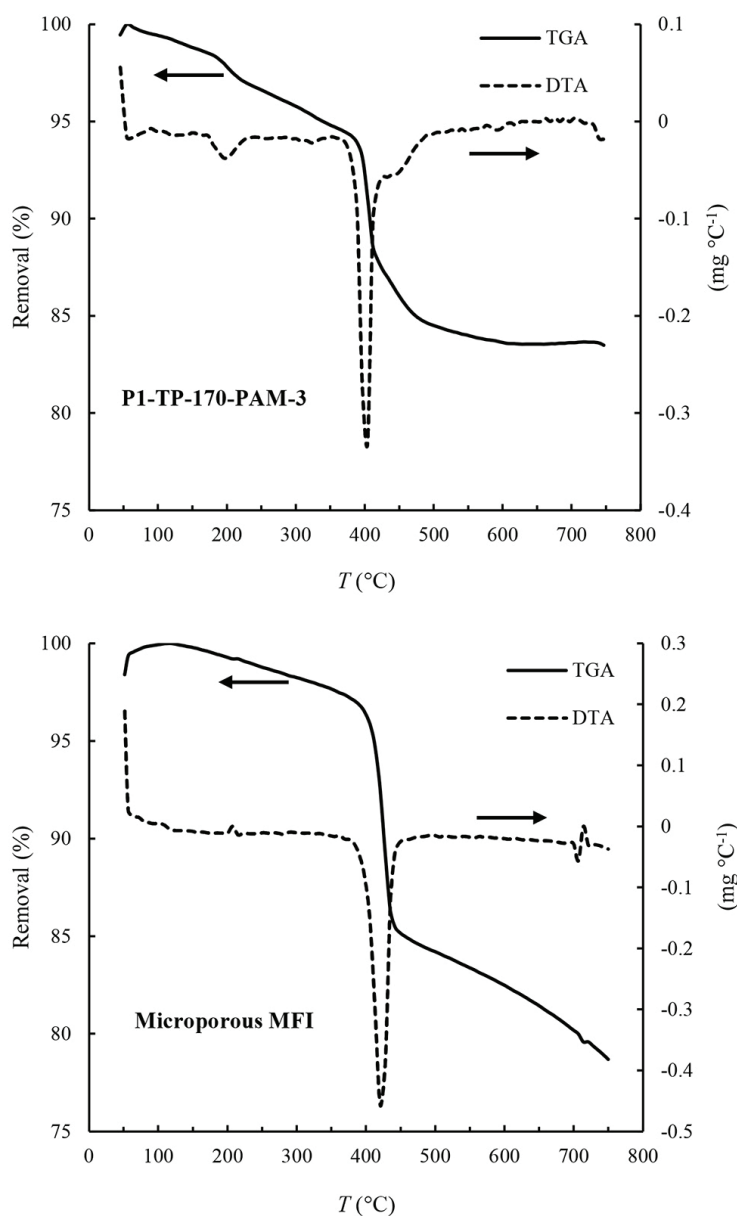| Membrane	S_{BET} (m² g⁻¹)	S_{Meso} (m² g⁻¹)	V_{Total} (cm³ g⁻¹)	V_{Meso} (cm³ g⁻¹)	V_{Micro} (cm³ g⁻¹)	Meso (%)
P1-TP-170-PAM-3	328.200	298.856	0.182	0.165	0.017	90.8
P2-TP-170-PAM-5	326.916	292.881	0.184	0.164	0.020	89.2

Fig. 3 – *DTG-TGA analysis of powder samples P1-TP-170-PAM-3 and microporous MFI zeolite*

nificant decomposition step at approximately 430 °C, continuing until approximately 450 °C. However, P1-TP-170-PAM-3, which contained the secondary template, underwent a major decomposition step at 400 °C and continued to decompose until approximately 500 °C. The initial decomposition at lower temperatures was due to the mesoporous structure within the zeolite, which allowed the rapid release of decomposition products (CO, CO_2, NO_X, NH_3

and H_2O). The decomposition up to 500 °C was also attributed to the remaining templates (secondary templates) in the structure. Furthermore, the absence of weight loss in P1-TP-170-PAM-3 at higher temperatures, compared to the decreasing weight trend in the microporous MFI zeolite powder, indicated a more stable structure. At high temperatures, zeolite structures can collapse and lose their structural water. Thus, selecting 550 °C for calcination of the synthesized powders and membrane was found to be suitable for membrane preparation.

TEM analysis was used to examine the morphology and structure of P1-TP-170-PAM-3 at various magnifications and to visualize the mesopores of the synthesized crystals. Figs. 4a and 4b show the hexagonal and coffin-like (MFI zeolite structure) structures associated with P1-TP-170-PAM-3. These images, along with the XRD results, confirm the MFI structure in the synthesized sample. Figs. 4c and 4d show the mesoporous structure of the calcined powder, consistent with the findings from BET analysis, confirming the mesoporous structure of the synthesized zeolite powder.

Characterization of the mesoporous MFI zeolite membrane

Fig. 5 shows the surface and cross-sectional FESEM images of M-TP-170-PAM-3. Low-magnification images provide information on the quality of the synthesized layer, while the high-magnification images reveal the morphology and structure of the zeolite crystals. Image (a) shows comprehensive coverage of the support surface by zeolite crystals. As the magnification increased, as shown in images (b) and (c), the hexagonal and coffin-like crystal structures became visible in the MFI zeolite. Images (d) and (e) present cross-sectional views of the synthesized membrane layer, which had a thickness of 7–9 μm. The surface roughness of the membrane layer indicated uneven crystal growth. In some regions of the support surface, nucleation occurred during synthesis, while in others, crystals underwent nucleation and further grow, resulting in increased roughness.

Fig. 6 shows the EDX-MAP analysis performed in conjunction with FESEM to assess the distribution of aluminum, oxygen, and silicon atoms in the synthesized membrane (M-TP-170-PAM-3). This analysis helped distinguish between the synthesized
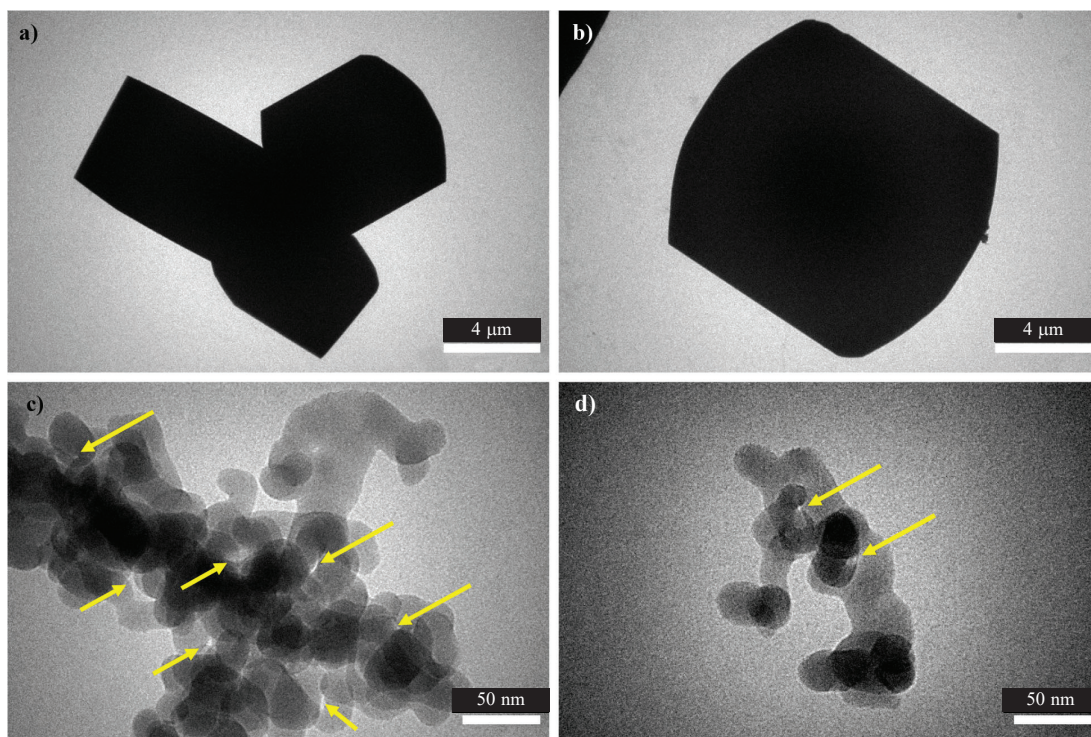
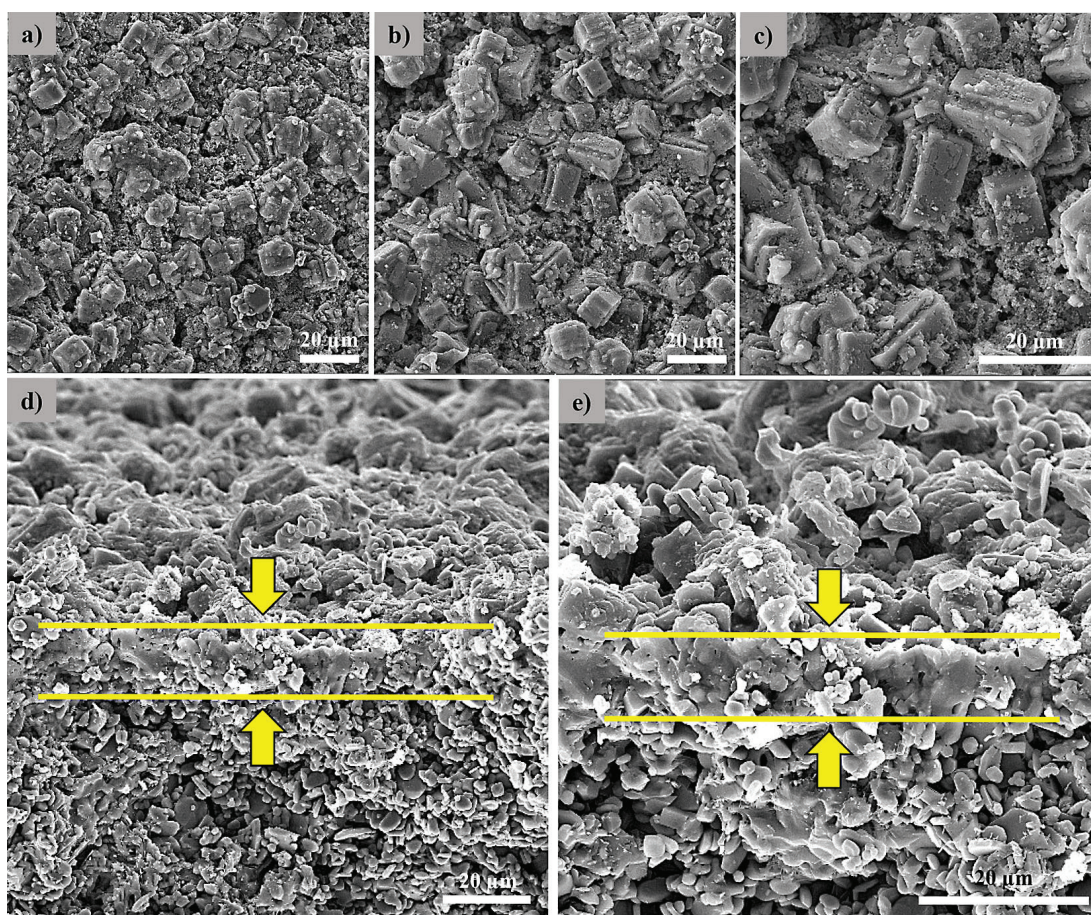F i g . 4 – *TEM images of sample P1-TP-170-PAM-3 at various magnifications*

F i g . 5 – *FESEM images of the surface (a, b, c) and cross-sectional surface (d, e) of the synthesized M-TP-170-PAM-3 membrane*
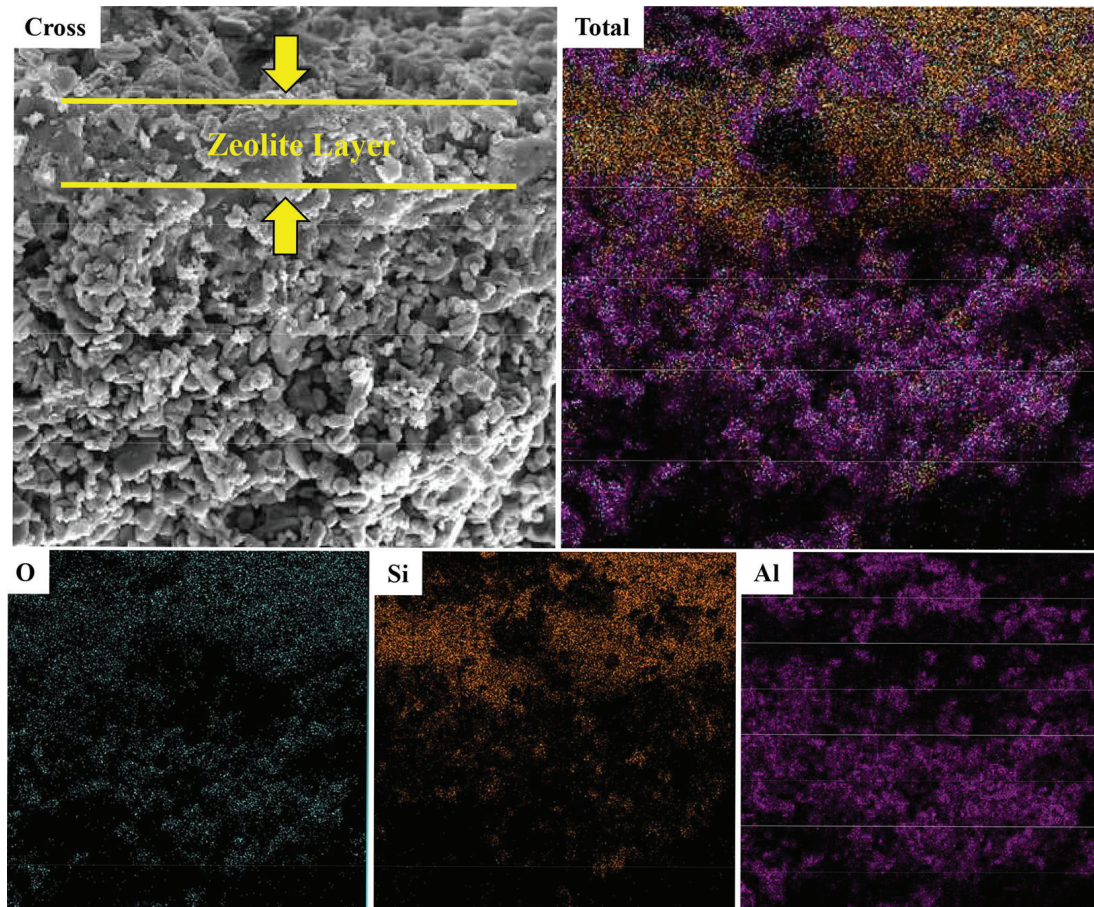
F i g . 6 – *EDX-MAP analysis of the cross-sectional surface of the mesoporous zeolite membrane M-TP-170-PAM-3*

membrane layer and its support. The presence of silicon atoms in the zeolite membrane layer was high, while aluminum atoms were more prevalent in the support. This was due to the formation of a silica-rich structure in the MFI zeolite layer and an aluminum-rich structure in the α-alumina support. Consequently, the density of silicon atoms decreased from the top (zeolite layer) to the bottom (α-alumina support), while the density of aluminum atoms increased.

Separation performance of the mesoporous MFI zeolite membrane

The separation performance of the synthesized mesoporous zeolite MFI membrane (M-TP-170-PAM-3) was evaluated using a water permeation test, along with the rejection of heavy metals and nitrate ions. Various factors influence the water permeation rate through the zeolite membrane, such as pressure and total dissolved solids (TDS). To investigate water permeation, two types of water feed were applied to the membrane module (deionized water with TDS = 1 $\mu A\ A^{-1}$, and natural water containing 145 $\mu A\ A^{-1}$ nitrates ions with TDS = 1000 $\mu A\ A^{-1}$). Due to the low flux at lower pressures for

the natural water, feed pressures of 6 and 8 bar were selected. Water permeation through the α-alumina substrate was also examined to determine the resistance created by the synthesis of the zeolite membrane layer. The results are presented in Table 2. The results of water permeation with TDS = 1 $\mu A\ A^{-1}$ through the synthesized membrane and the α-alumina substrate indicate that the mass transfer resistance increased when the zeolite MFI layer was synthesized on the substrate, leading to a reduction in pore size. A water permeation test with a high TDS (TDS = 1000 $\mu A\ A^{-1}$) revealed that the permeation rate for water containing solids and various ions was higher than that for water with a low TDS. The presence of different ions in natural water can enhance the wettability of the zeolite membrane surface by affecting the density of polar hydroxyl groups and the physical and chemical properties of pore surfaces. This explains the higher flux observed with the natural water feed; increasing the surface hydrophilicity of zeolite membranes increases their water permeation rate[21]. The water permeation rates reported in Table 2 were measured after 2 h, and the details of the water permeation rate over time are shown in Fig. 7. As the feed pres-

Table 2 – *Water permeation through the synthesized membrane (M-TP-170-PAM-3) and α-alumina support at different pressures*

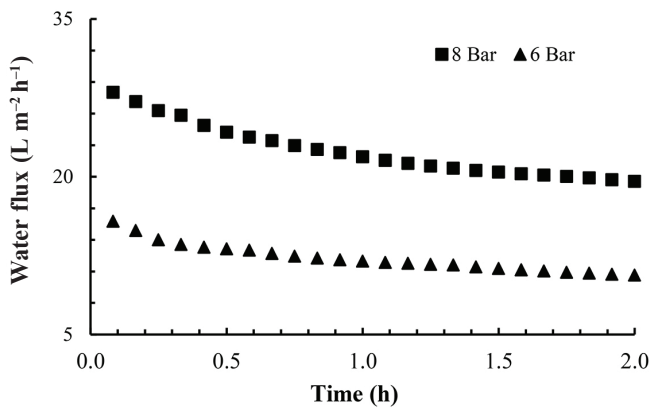| Sample	Water (TDS = 1 μA A^{-1})		Water containing nitrates (TDS = 1000 μA A^{-1})	
Pressure	6	8	6	8
M-TP-170-PAM-3 (L m^{-2} h^{-1})	10	15	12.5	22.44
Support (L m^{-2} h^{-1})	608	717	–	–

Fig. 7 – *Permeation of natural water containing nitrate ions (145 μA A^{-1}) through the synthesized membrane (M-TP-170-PAM-3) at 6 and 8 bar pressures*

sure or driving force increased, the interaction between molecules and the membrane surface intensified, leading to a higher water permeation rate. Furthermore, increased pressure contributed to greater membrane fouling. The reduction in water permeation at 8 and 6 bar was approximately 5.5 L m^{-2} h^{-1} and 3 L m^{-2} h^{-1}, respectively. The greater reduction at 8 bar can be attributed to the blockage of small pores by solids in the water under higher applied force. At low feed pressures, solids are unable to enter small pores, allowing only water molecules to permeate through them. However, as pressure increases, small solids can enter and block the pores.

Aqueous solutions containing nickel, chromium, and nitrate ions were used to evaluate the performance of the synthesized membrane (M-TP-170-PAM-3) in separating these ions from water. The nitrate solution consisted of natural water containing 145 μA A^{-1} nitrate ions with TDS = 1000 μA A^{-1}. Nickel and chromium solutions were prepared by dissolving appropriate amounts of Ni(NO$_3$)$_2$ and Cr(NO$_3$)$_3$ in water, with the water used in these preparations having a TDS level of 1 μA A^{-1}. Sampling was conducted after 30 min of flow through the membrane. The different ion rejection rates of the synthesized membrane are shown in Fig. 8. The order of the hydrated radius of the tested ions was Ni^{2+} > Cr^{3+} > NO$_3^-$. Due to the smaller hydrated radius of nitrate ions, they exhibited lower rejection by the membrane. Chromium ions, with a slightly smaller hydrated radius than nickel ions, also showed lower rejection compared to nickel ions. The rejection rate was 99 % for nickel ions and 93 % for chromium ions at different pressures. In contrast, the rejection rate for nitrate ions was 34 % under the highest pressure conditions. Increasing the pressure did not significantly affect the membrane's rejection of nickel or chromium ions, as their large hydrated radii prevented their entrance into the membrane pores even at high pressures. However, the rejection of nitrate ions increased with higher pressure, likely due to increased fouling of the membrane pores by impurities present in the natural water feed with TDS = 1000 μA A^{-1} (Natu-

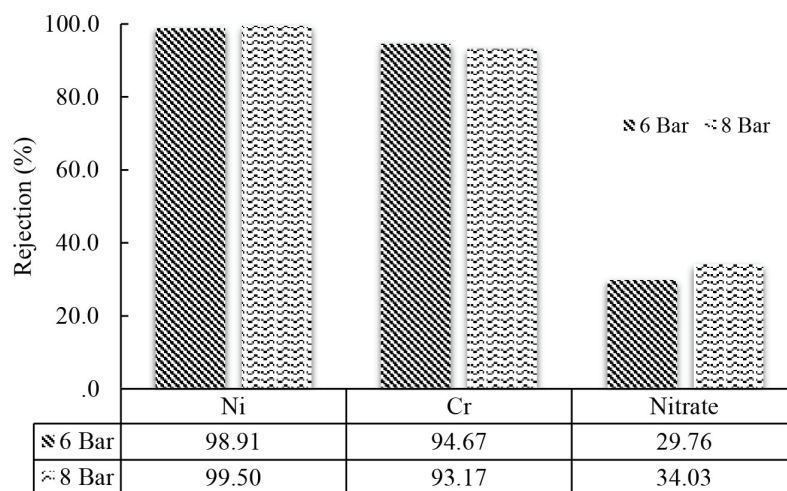|	Ni	Cr	Nitrate
6 Bar	98.91	94.67	29.76
8 Bar	99.50	93.17	34.03

Fig. 8 – *Rejection of nitrate ions and heavy metal ions (nickel and chromium) in an aqueous solution by the membrane (M-TP-170-PAM-3) at pressures 6 and 8 bar*

ral-source water has a variety of naturally occurring substances, including metals, minerals, nutrients, organic matter and microorganisms). As a result, water permeation through the membrane decreased with rising pressure, leading to increased ion rejection.

Conclusion

The use of polyacrylamide as a soft secondary template in the synthesis of MFI zeolite is an easy method for creating a mesoporous structure within MFI zeolite. However, a higher polymer content does not enhance pore size and may actually hinder the formation of zeolite structures. On the other hand, incorporating a small amount of polyacrylamide (0.03 kg kg^{-1} dry precursors) into the MFI zeolite synthesis solution can generate a high mesopore content (90 %) within the MFI zeolite. This method resulted in the synthesis of a mesoporous MFI zeolite membrane with high water flux (22 L m^{-2} h^{-1}) and excellent rejection of heavy metal ions (99 % nickel and 93 % chromium) from water. Water permeation analysis indicated that an increase in total dissolved solids (TDS) in water had a positive effect on increasing water permeability (by 50 %). Additionally, increasing the feed pressure led to increased water flux, membrane fouling, and ion rejection by the membrane.

References

1. *Yahaya, Y. A., Don, M. M.,* Pycnoporus sanguineus as a potential biosorbent for heavy metal removal from aqueous solution: A review, J. Phys. Sci. **25**(1) (2014) 1.
https://api.semanticscholar.org/CorpusID:138679945

2. *Emenike, P. C., Omole, D. O., Ngene, B. U., Tenebe, I. T.,* Potentiality of agricultural adsorbent for the sequestering of metal ions from wastewater, Glob. J. Environ. Sci. Manag. **2**(4) (2016) 411.
doi: https://doi.org/10.22034/gjesm.2016.02.04.010

3. *Algieri, C., Drioli, E.,* Zeolite membranes: Synthesis and applications, Sep. Purif. Technol. **278** (2021) 119295.
doi: https://doi.org/10.1016/j.seppur.2021.119295

4. *Khajavi, S., Jansen, J. C., Kapteijn, F.,* Production of ultra-pure water by desalination of seawater using a hydroxy sodalite membrane, J. Memb. Sci. **356**(1–2) (2010) 52.
doi: https://doi.org/10.1016/j.memsci.2010.03.026

5. *Xia, S., Peng, Y., Wang, Z.,* Microstructure manipulation of MFI-type zeolite membranes on hollow fibers for ethanol-water separation, J. Memb. Sci. **498** (2016) 324.
doi: https://doi.org/10.1016/j.memsci.2015.10.024

6. *Cho, C. H., Oh, K. Y., Kim, S. K., Yeo, J. G., Sharma, P.,* Pervaporative seawater desalination using NaA zeolite membrane: Mechanisms of high water flux and high salt rejection, J. Memb. Sci. **371**(1–2) (2011) 226.
doi: https://doi.org/10.1016/j.memsci.2011.01.049

7. *Shu, X., Wang, X., Kong, Q., Gu, X., Xu, N.,* High-flux MFI zeolite membrane supported on YSZ hollow fiber for separation of ethanol/water, Ind. Eng. Chem. Res. **51**(37) (2012) 12073.
doi: https://doi.org/10.1021/ie301087u

8. *Drobek, M., Yacou, C., Motuzas, J., Julbe, A., Ding, L., Diniz da Costa, J. C.,* Long-term pervaporation desalination of tubular MFI zeolite membranes, J. Memb. Sci. **415–416** (2012) 816.
doi: https://doi.org/10.1016/j.memsci.2012.05.074

9. *Zhou, C., Zhou, J., Huang, A.,* Seeding-free synthesis of zeolite FAU membrane for seawater desalination by pervaporation, Microporous Mesoporous Mater. **234** (2016) 377.
doi: https://doi.org/10.1016/j.micromeso.2016.07.050

10. *Wang, L., Yang, J., Wang, J., Raza, W., Liu, G., Lu, J., Zhang, Y.,* Microwave synthesis of NaA zeolite membranes on coarse macroporous α-Al$_2$O$_3$ tubes for desalination, Microporous Mesoporous Mater. **306** (2020) 110360.
doi: https://doi.org/10.1016/j.micromeso.2020.110360

11. *Chen, F., Li, Y., Huang, A.,* Facile preparation of compact LTA molecular sieve membranes on polyethyleneimine modified substrates, Chinese Chem. Lett. **32**(3) (2021) 1086.
doi: https://doi.org/10.1016/j.cclet.2020.07.047

12. *Wang, Y., Rong, H., Sun, L., Zhang, P., Yang, Y., Jiang, L., Wu, Sh., Zhu, G., Zou, X.,* Fabrication and evaluation of effective zeolite membranes for water desalination, Desalination **504** (2021) 114974.
doi: https://doi.org/10.1016/j.desal.2021.114974

13. *Van Oers, C. J., Stevens, W. J. J., Bruijn, E., Mertens, M., Lebedev, O. I., Van Tendeloo, G., Meynen, V., Cool, P.,* Formation of a combined micro- and mesoporous material using zeolite Beta nanoparticles, Microporous Mesoporous Mater. **120**(1–2) (2009) 29.
doi: https://doi.org/10.1016/j.micromeso.2008.08.056

14. *Verboekend, D., Pérez-Ramírez, J.,* Desilication mechanism revisited: Highly mesoporous all-silica zeolites enabled through pore-directing agents, Chem. Eur. J. **17**(4) (2011) 1137.
doi: https://doi.org/10.1002/chem.201002589

15. *Ogura, M., Shinomiya, Sh., Tateno, J., Nara, Y., Nomura, M., Kikuchi, E., Matsukata, M.,* Alkali-treatment technique – New method for modification of structural and acid-catalytic properties of ZSM-5 zeolites, Appl. Catal. A Gen. **219**(1–2) (2001) 33.
doi: https://doi.org/10.1016/S0926-860X(01)00645-7

16. *Zhang, H., bin Samsudin, I., Jaenicke, S., Chuah, G. K.,* Zeolites in catalysis: Sustainable synthesis and its impact on properties and applications, Catal. Sci. Technol. **12**(19) (2022) 6024.
doi: https://doi.org/10.1039/D2CY01325H

17. *Singh, B. K., Kim, Y., Kwon, S., Na, K.,* Synthesis of mesoporous zeolites and their opportunities in heterogeneous catalysis, Catalysts **11**(12) (2021) 1541.
doi: https://doi.org/10.3390/catal11121541

18. *Abdulridha, S., Jiao, Y., Xu, Sh., Zhang, R., Ren, Zh., Garforth, A. A.,* A comparative study on mesoporous Y zeolites prepared by hard-templating and post-synthetic treatment methods, Appl. Catal. A Gen. **612** (2021) 117986.
doi: https://doi.org/10.1016/j.apcata.2020.117986

19. *Meng, X., Nawaz, F., Xiao, F. S.,* Templating route for synthesizing mesoporous zeolites with improved catalytic properties, Nano Today **4**(4) (2009) 292.
doi: https://doi.org/10.1016/j.nantod.2009.06.002

20. *Dubey, M., Wadhwa, S., Mathur, A., Kumar, R.,* Progress in mesoporous ceria: A review on synthesis strategies and catalytic applications, Appl. Surf. Sci. Adv. **12** (2022) 100340.
doi: https://doi.org/10.1016/j.apsadv.2022.100340

21. *Wang, Y., Rong, H., Sun, L., Zhang, P., Yang, Y., Jiang, L., Wu, Sh., Zhu, G., Zou, X.,* Fabrication and evaluation of effective zeolite membranes for water desalination, Desalination **504** (2021) 114974.
doi: https://doi.org/10.1016/j.desal.2021.114974